# Direct Measurement of Length Scale Dependence of the Hydrophobic Free Energy of a Single Collapsed Polymer Nanosphere

Weishuai Di,[1] Xiang Gao,[1] Wenmao Huang,[1] Yang Sun,[1] Hai Lei,[1] Yang Liu,[1] Wenfei Li,[1,2] Yiran Li,[1] Xin Wang,[1] Meng Qin,[1] Zhenshu Zhu,[1,*] Yi Cao,[1,2,†] and Wei Wang[1,2,‡]

[1]*Collaborative Innovation Center of Advanced Microstructures, National Laboratory of Solid State Microstructure, Department of Physics, Nanjing University, Nanjing 210093, People's Republic of China*

[2]*Institute for Brain Sciences, Nanjing University, Nanjing 210023, People's Republic of China*

(Received 15 June 2018; revised manuscript received 15 November 2018; published 31 January 2019)

The physics underlying hydrophobicity at macroscopic and microscopic levels is fundamentally distinct. However, experimentally quantifying the length scale dependence of hydrophobicity is challenging. Here we show that the size-dependent hydrophobic free energy of a collapsed polymer nanosphere can be continuously monitored from its single-molecule force-extension curve using a novel theoretical framework. The hydrophobic free energy shows a change from cubic to square dependence of the radius of the polymer nanosphere at a radius of ~1 nm—this is consistent with Lum-Chandler-Weeks theory and simulations. We can also observe a large variation of the hydrophobic free energy of each polymer nanosphere implying the heterogeneity of the self-assembled structures and/or the fluctuation of the water-polymer interface. We expect that our approach can be used to address many fundamental questions about hydrophobic hydration, which are otherwise inaccessible by ensemble measurements.

DOI: 10.1103/PhysRevLett.122.047801

Hydrophobic interactions underlie many biological self-assembly processes including protein folding and assembly, ligand-receptor binding, as well as micelle and membrane formation [1–8]. Theoretical work pioneered by Stillinger [9] and significantly elaborated by Lum *et al.* [10] has highlighted the distinct mechanisms for the hydrophobic hydration of small solutes and larger ones. Small solutes can be incorporated into surrounding water molecules by simple entropy-driven fluctuations of water; the solvation of larger solutes requires the formation of hydrophobic-hydrophilic interface and is an enthalpy-dominated process.

The length scale dependence at which the crossover of the two hydrophobic hydration mechanisms occurs is critical for the hydrophobic interaction mediated processes. Following the model proposed by Lum *et al.*, a series of simulation works on hydrophobic solutes of various size have confirmed that the free energy crossover occurs at a radius of ~1 nm [11–14]. Moreover, they found that the solute-solvent attraction can affect the water structure around the solutes in a size-dependent fashion [15,16]. Therefore, the crossover length is dependent not only on the chemical properties of solutes but also on the solvent conditions [6,17].

Experimentally, verification of the length scale dependence of hydrophobic free energy has been challenging [18]. For small solutes, the hydrophobic free energy was typically quantified by measuring the transfer free energy from a nonpolar solvent to water [19] or more precisely from the gas phase to water [20,21]. However, hydrophobic polymers are insoluble in water, and the solvation free energy cannot be experimentally evaluated from the solubility data.

Ben-Amotz and co-workers initiated direct measurement of hydrophobic hydration shells using Raman scattering [22]; however, the hydration of collapsed polymers has not yet been revealed. Recently, Li and Walker introduced a method to measure the solvation free energy of the monomer units of hydrophobic homopolymers using atomic-force-microscopy-(AFM) based single-molecule force spectroscopy (SMFS) [23–26]. In this approach, single collapsed polymer nanospheres were unfolded and extended by tensile force. The hydration free energy of the monomer units can be estimated based on the plateau force of the force-extension curves. They found that the hydration of a monomer unit in the polymer is different from a free monomer [24]. The temperature-dependent hydration free energy profiles of the polymers correlate with the size of the monomer units at the subnanometer scale [24] and are consistent with predictions from the Lum-Chandler-Weeks theory. However, the length scale dependence of free energy of the collapsed nanosphere was not considered. Such collapsed nanospheres somewhat resembled the molten globular structures of proteins and were extensively used as a model system to understand the hydrophobic collapse, as this was the major driving force for protein folding [27,28]. This suggests that the free energy of such compact nanospheres formed solely by hydrophobic collapse can provide significant insights into many biological processes driven by hydrophobic interactions including protein folding and self-assembly of various macromolecules.

Inspired by the above work, we show here that the free energy of the collapsed polymer nanospheres can be directly derived from SMFS experiments with high-quality

 

force-extension data and a new theoretical model. Previous experiments relied on nonspecific attachment of the polymer to either the cantilever tip or the substrate. The dangling ends of the polymers outside the anchoring sites may introduce additional interactions to the stretched polymers [23,24]. Therefore, the region corresponding to the globule-to-coil transition in the force spectroscopy (the very end of the force plateau) cannot be reliably measured. In our approach, the two ends of the hydrophobic polymers were covalently linked to the cantilever tip and the substrate, respectively; nonspecific interactions were significantly reduced. We also provided a theoretic framework to reconstruct the free energy landscape for the unfolding of the collapsed polymer nanospheres. Our results indicated that the hydrophobic free energy of PS nanosphere scales with their volume at the radius less than 1 nm and with their surface area at larger radius.

We first employed SMFS to study the unfolding behavior of collapsed single-chain PS nanospheres in deionized water [Fig. 1(a)]. We synthesized a bifunctional PS polymer ($M_n$, 117 kDa; polydispersity, 1.59; see the Supplemental Material 2.1–2.4 and Fig. S2 for details [29]) to anchor the two ends of the PS polymers to the cantilever tip and the substrate. The polymers were covalently linked to the azide-functionalized glass substrate via Staudinger ligation. When immersing the substrate in deionized water, the surface-tethered PS polymers collapsed into single-chain nanospheres with an average height of ~4 nm [Fig. 1(b)] as seen by AFM imaging. As the glass surfaces were hydrophilically treated and functionalized with azide groups, the nonspecific adsorption of PS polymers to the surfaces was greatly reduced. (See the Supplemental Material 2.5 for details [29]). Next, the maleimide-functionalized cantilever tip was brought into contact with the surface to fish the thiol group at the other end of the polymer. The maleimide-coated cantilever tip can reduce the nonspecific interactions between the tip and the PS polymers. In addition, we used low contact force of 500–800 pN and short contact time of 0.5–1 s to minimize the chance of picking up PS polymers nonspecifically and to ensure most events corresponding to covalent linkage (see the Supplemental Material 2.6 for details [29]). Subsequently, the polymer nanosphere was stretched resulting in a force-extension curve with a representative force plateau at ~80 pN [Fig. 1(c)]. This region corresponds to gradually stretching the PS chain from the nanosphere [23,24]. The very end of the force plateau corresponds to the changing of the nanosphere with a size of a few nanometers to a completely unfolded single chain (globule-to-coil transition) covering the crossover region of hydrophobicity. When the nanosphere was fully stretched, the extended PS chain in water behaved similar to a hydrophilic polymer under force. This region can be fitted using a WLC model of polymer elasticity [42].

To confirm that the force plateau was indeed due to hydrophobic collapse, we performed control SMFS

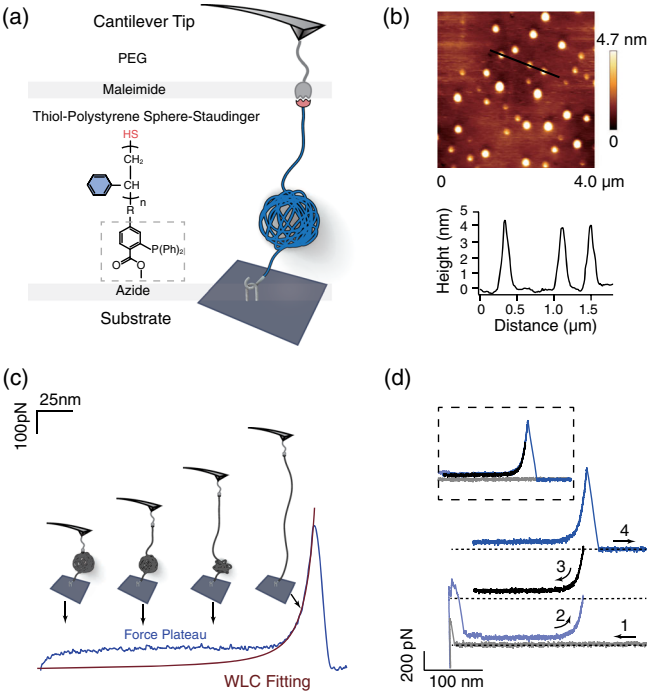


FIG. 1. SMFS experiment of stretching a collapsed hydrophobic polystyrene (PS) nanosphere. (a) Schematic diagram of the experimental design. (b) AFM image of the PS nanospheres covalently deposited on the glass surface. The height profile of the marked line is shown below. (c) A representative force-extension curve for the unfolding of the collapsed PS nanosphere. The red line corresponds to wormlike chain (WLC) fitting of the stretching of this unfolded chain. Snapshots of different experimental stages are shown as the insets. (d) Typical unfolding or refolding curves of the PS nanosphere. (1) The cantilever was approached towards the substrate to capture the free thiol at the end of the PS nanosphere. (2) The cantilever was retracted to stretch the polymer to a fully unfolded structure. (3) The polymer was relaxed to a position close to the surface. (4) The polymer was fully stretched again till ruptured. The overlap of the stretching and relaxation curves (inset) indicates that the unfolding or refolding is a reversible quasistatic process.

experiments in a good solvent [toluene, Fig. S4(a) in the Supplemental Material [29] ]. The full range of the force-extension curves can be fitted using either the WLC model or freely jointed chain (FJC) model; no force plateaus were detected indicating that the PS polymer behaved like an entropic spring without hydrophobic collapse. For long polymer chains, the chain entanglement can lead to additional friction of the chains upon stretching. However, we did not observe any obvious change of the plateau forces at the pulling speeds below 4000 nm/s (see Fig. S5 in the Supplemental Material [29]) suggesting that the entangled chains have sufficient time to rearrange and disentangle under our experimental conditions [43,44]. Only in extreme cases does the entangled chain form knots (see Fig. S6 in the Supplemental Material [29]); those data were excluded in the data analysis.

Next, to investigate whether the unfolding of PS nanosphere is reversible, we performed stretching-relaxation experiments [Fig. 1(d)]. A PS nanosphere was picked up and stretched to ~500 pN to produce the fully unfolded PS polymer while avoiding detachment. The polymer was then relaxed to a shorter extension to allow nanosphere refolding. The relaxation curve shows a similar force plateau as the first stretching curve suggesting that the nanosphere formed instantly when force was relaxed, and the unfolding or refolding of the PS nanosphere is a quasistatic process. Therefore, the next stretching curve also shows the same feature as the first one; all stretching and relaxation curves are superimposable. As such, the free energy change of the entire process can be directly calculated from the mechanical work measured experimentally.

Next, we derived a theoretical model to quantify the change of the free energy based on the force-extension curves. As shown in Fig. 2(a), the hydration free energy of the total PS polymer ($G$) during the stretching comprises three parts: the hydration free energy of the compacted nanosphere ($G_{\mathrm{sph}}$), the hydration free energy of the stretched PS chain ($G_{\mathrm{chain}}$), and the conformational entropy of the polymer chain ($G_{\mathrm{WLC}}$):

$$G(x, L, R) = G_{\mathrm{sph}}(R) + G_{\mathrm{chain}}(L) + G_{\mathrm{WLC}}(x, L). \quad (1)$$

Here, $G_{\mathrm{sph}}$ is solely a function of the radius of the PS nanosphere $R$. $G_{\mathrm{chain}}$ is proportional to the contour length of the stretched chain $L$, and $G_{\mathrm{chain}}(L) = \mu_C L$, where $\mu_C$ is the hydrophobic hydration free energy per contour length of the chain. The elasticity of the unfolded PS chain is described by the WLC model [42]:

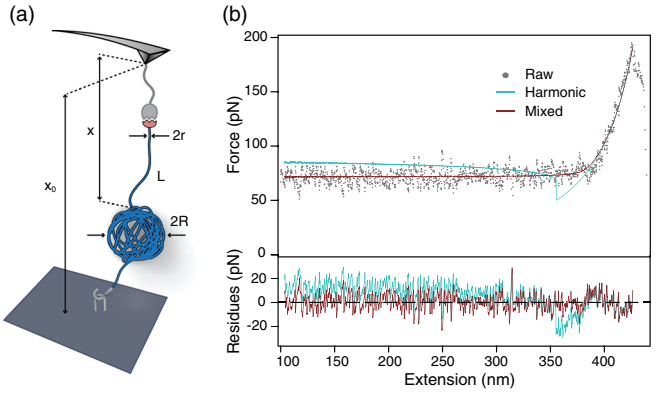


FIG. 2. Theoretical model and numerical simulation. (a) Schematic illustration of the theoretical model and all parameters in the equations. (b) The force-extension curve and the simulated curves based on different theoretical models. Harmonic model: The free energy of $G_{\mathrm{sph}}(R)$ containing only the quadratic term. Mixed model: The free energy of $G_{\mathrm{sph}}(R)$ containing both the quadratic and the cubic terms.

$$F = \frac{1}{4\beta L_p}\left[\left(1 - \frac{x}{L}\right)^{-2} - 1 + \frac{4x}{L}\right], \quad (2)$$

where $\beta = 1/k_B T$ ($k_B$ is the Boltzmann constant and $T$ is the temperature in kelvin), $L_p$ is the persistence length, $L$ is the contour length of the stretched chain, and $x$ is the end-to-end distance. Since $F = \partial G_{\mathrm{WLC}}(x, L)/\partial x$, we get

$$G_{\mathrm{WLC}}(x, L) = \frac{1}{4\beta L_p}\frac{x^2(3L - 2x)}{L(L - x)}. \quad (3)$$

$G_{\mathrm{WLC}}(x, L)$ can be directly obtained by fitting the WLC region of the curve. Therefore, Eq. (1) can be rewritten as

$$G(x, L, R) = G_{\mathrm{sph}}(R) + \mu_C L + \frac{1}{4\beta L_p}\frac{x^2(3L - 2x)}{L(L - x)}. \quad (4)$$

There are also two constraints in the system: The total volume, $V_0 = 4\pi/3R_0^3$ ($V_0$ is the initial volume and $R_0$ is the initial radius of the PS nanosphere) and the total end-to-end distance of the polymer or the distance between the cantilever tip and the substrate $X_0$,

$$\frac{4\pi}{3}R_0^3 = \frac{4\pi}{3}R^3 + \pi r^2 L, \quad (5)$$

$$X_0 = x + 2R. \quad (6)$$

Here, $r$ is the radius of the polymer chain corresponding to the size of the polymer unit; $R$ and $x$ are the radius of the nanosphere and the end-to-end distance of the elongated polymer chain outside the nanosphere, respectively [Fig. 2(a)].

Because the unfolding or refolding of the nanosphere is reversible, $dG = 0$. The only unknown term in Eq. (4) is $G_{\mathrm{sph}}(R)$. We can simulate the force-extension curves by assuming different types of $G_{\mathrm{sph}}(R)$ to test whether the shape of the force-extension curve is sensitive to the free energy profiles of the nanosphere (see the Supplemental Material 2.8.1 for details [29]).

In the previous model derived by Li and Walker, $G_{\mathrm{sph}}(R)$ only contains the interfacial energy and is proportional to the surface area [23]. Therefore, $G_{\mathrm{sph}}(R)$ is a harmonic potential with a quadratic function (harmonic model). Although the harmonic model can reproduce the force plateau region reasonably well, it failed to match the crossover region [Fig. 2(b)]. According to the Lum-Chandler-Weeks theory, $G_{\mathrm{sph}}(R)$ contains both the enthalpic and the entropic terms [10]. The entropy of the hydration of small hydrophobic solutes depends on their volume and thus is a cubic function of the radius; however, enthalpy depends on their surface area and thus is a quadratic function.

We then tested whether the full force-extension curve can be replicated by the theory that includes both the quadratic and the cubic functions to $G_{\mathrm{sph}}(R)$ (mixed model). Clearly, the mixed model can reproduce experimental data reasonably well for both the force plateau, the globule-to-coil transition, and the WLC regions [Fig. 2(b)]. Fitting errors here are less than the noise level of the force-extension curves (~10 pN). Therefore, it is possible to distinguish the hydrophobic hydration mechanism based on the force-extension curves.

We further endeavored to obtain $G_{\mathrm{sph}}(R)$ directly from experimental data without any preset models. Since the unfolding of the PS nanosphere is a quasistatic process, the $G_{\mathrm{sph}}(R)$ can be calculated via the Lagrange multiplier to find the extreme point of the total free energy in Eq. (4) subjected to two equality constraints shown in Eqs. (5) and (6) (see the Supplemental Material 2.8.2 for details [29]). The relationship between the derivative of $G_{\mathrm{sph}}(R)$ and experimental data follows

$$\frac{dG_{\mathrm{sph}}}{dR} = 2F + \frac{4R^2}{r^2}\left(\mu_C + \frac{\partial G_{\mathrm{WLC}}}{\partial L}\right), \tag{7}$$

where $F$ is the force from the force-extension curves, and the other parameters are as defined previously. $r$ can be obtained based on the chemical structure of the monomer unit. The rest of the parameters in Eq. (7) can be directly obtained from the experimentally measured force-extension curves. Therefore, integrating Eq. (7) yields the free energy profiles of the PS nanospheres,

$$\Delta G_{\mathrm{sph}} = \int_0^{R_0} \frac{dG_{\mathrm{sph}}}{dR'} dR'. \tag{8}$$

Converting experimentally determined force-extension curves to free energy profiles using Eqs. (7) and (8) does not need any preknowledge of the shape of the free energy profile. The reconstructed free energy landscapes using Eq. (8) from 39 different force-extension curves are summarized in Fig. 3(a). While there are big variations in the free energy change, they show similar trends. The red dotted line represents the average free energy profile.

The variation of the free energy grows with the radius $R$. This is consistent with the prediction from the capillary-wave theory [45,46]. In the theory, the fluctuation of the water-solid interface is controlled by the reverse work of the surface tension. Therefore, the square of the interface width $z^2$ shows a linear dependence with the logarithm of the radius $R$:

$$z^2 = z_0^2 + \frac{\beta}{2\pi\lambda}\ln\left(\frac{R}{B_0}\right). \tag{9}$$

Here, $z_0$ is the intrinsic interfacial width, $B_0$ is a short wavelength cutoff set by the size of the nanosphere ($B_0$ of 1 nm is used in the calculation), $\lambda$ is the interfacial tension, and $\beta$ is as defined previously. Because of the fluctuation of the water-solid interface, the free energy varies more at larger $R$ values. According to Eq. (7) and the error propagation formula, the standard deviation of $\Delta G_{\mathrm{sph}}$, or $\Delta(\Delta G_{\mathrm{sph}})$, is proportional to $R^2 z$ and thus proportional to $R^2(\ln R)^{1/2}$. The plot of $\Delta(\Delta G_{\mathrm{sph}})$ with respect to $R^2(\ln R)^{1/2}$ is shown in the inset of Fig. 3(a). The linear relationship verifies the dynamic structures of the PS nanospheres predicted by capillary-wave theory.

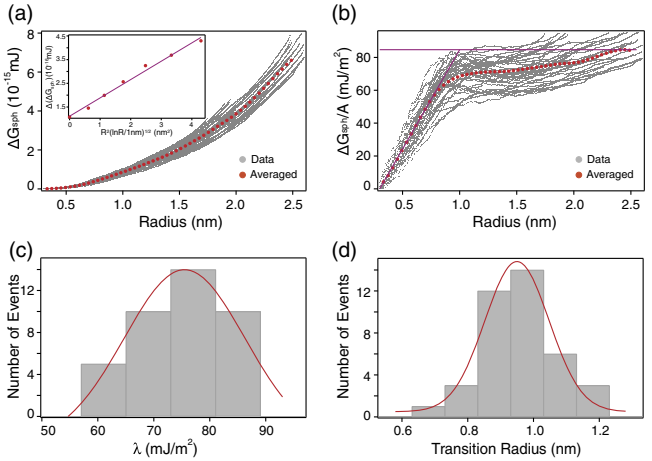


FIG. 3. Direct reconstruction of the free energy landscape for the hydrophobic hydration of the PS nanosphere from the experimental data. (a) The hydration free energy ($\Delta G_{\mathrm{sph}}$) determined from force-extension curves at different radii ($R$). Gray curves were calculated from 39 single-molecule events, and the red dotted line represents the averaged trace. The inset shows the standard deviation of the hydration free energy at $R > 1$ nm, $\Delta(\Delta G_{\mathrm{sph}})$, which is linearly dependent on $R^2(\ln R)^{1/2}$. (b) The hydration free energy per surface area $[(\Delta G_{\mathrm{sph}})/A, A = 4\pi R^2]$ at different radii. The red dotted line is the averaged trace. Two purple lines highlight the transitional behavior. (c) The histogram of the surface tension coefficient ($\lambda$). Gaussian fitting (red) measures an average $\lambda$ of $75.5 \pm 10.8$ mJ/m$^2$. (d) The histogram of the crossover radii. Gaussian fitting (red) measures an average crossover radius of $0.95 \pm 0.10$ nm.

Assuming that the PS nanosphere is a perfect sphere, we can plot the hydration free energy per surface area $(\Delta G_{\mathrm{sph}})/A$ with respect to the radius [Fig. 3(b)]. Clearly, when the radius is less than 1 nm, $(\Delta G_{\mathrm{sph}})/A$ is proportional to the radius of the nanosphere indicating that the free energy is a function dominated by a cubic expression of the radius. Therefore, in this region, the hydrophobic hydration is an entropy-driven process. However, when the radius is larger than 1 nm, $(\Delta G_{\mathrm{sph}})/A$ clearly deviates from the predicted entropy-driven process and gradually reaches a plateau. This suggests that $(\Delta G_{\mathrm{sph}})/A$ turns to a quadratic function of the radius, and the hydrophobic hydration becomes an enthalpy-driven process similar to the hydration of bulk hydrophobic objects [5,6]. Note that when force is applied, the PS nanosphere may be distorted to ellipsoid leading to an increase in the surface area (see Fig. S7 in the Supplemental Material [29]). We found that this effect only leads to an ~2.9% increase in the surface

area and does not strongly affect the estimated $(\Delta G_{\mathrm{sph}})/A$ (Supplemental Material 2.12 [29]).

Our approach provides an efficient means to experimentally determine the hydrophobic hydration free energy at the single-molecule level. The surface tension coefficients $\lambda$ taken as the asymptotic values of $(\Delta G_{\mathrm{sph}})/A$ when $R$ approaches infinity [Fig. 3(c)]. Gaussian fitting indicates that the expected value is $75.5 \pm 10.8\ \mathrm{mJ/m^2}$, which is slightly higher than that from microscopic calculation [11]. The discrepancy may result from the underestimated surface area using the perfect sphere assumption of the collapsed PS nanoparticle. Moreover, despite the large variation of $\lambda$, the crossover length shows a narrow distribution and is centered at $0.95 \pm 0.10$ nm [Fig. 3(d)] suggesting that the crossover of the hydrophobic hydration mechanism is independent of the fluctuation of the hydrophobic free energy.

We also derived the hydration free energy using the FJC model rather than the WLC model to describe the chain elasticity of the PS polymer. This ensures that the calculated hydration free energy and the crossover length are independent of the particular model of polymer elasticity (Supplemental Material 2.9.2 and Fig. S8 [29]).

In summary, we provide a convenient and practical way to quantitatively measure the hydrophobic free energy of collapsed polymers based on SMFS experiments. The calculated free energy profiles of collapsed PS nanospheres quantitatively agree well with the prediction from the Lum-Chandler-Weeks theory and previous simulations. Moreover, the hydrophobic free energy varies markedly among different molecules at the single-molecule level, which is consistent with the prediction from the capillary-wave theory. Our method enables measurement of the hydrophobicity of various biomacromolecules and assesses the impact of various biological conditions on hydrophobic hydration. These studies will further bridge the gap between experiments and theory and improve our understanding of the physical mechanisms of hydrophobicity.

We thank Dr. Gilbert C. Walker, Jie Yan, and Isaac T. S. Li for discussions, and Dr. Zuoxiu Tie for GPC measurements. This work was financially supported by NSFC Grants No. 21522402, No. 21774057, No. 11674153, and No. 11334004, the Priority Academic Program Development (PAPD) of Jiangsu Higher Education Institutions, and the Fundamental Research Funds for the Central Universities (Grants No. 14380080, No. 14380098, and No. 14380090).

W. D., X. G., and W. H. contributed equally to this work.

*Corresponding author.
zhuzhenshu@163.com
†Corresponding author.
caoyi@nju.edu.cn
‡Corresponding author.
wangwei@nju.edu.cn

[1] B. J. Berne, J. D. Weeks, and R. H. Zhou, Annu. Rev. Phys. Chem. **60**, 85 (2009).
[2] S. N. Jamadagni, R. Godawat, and S. Garde, Annu. Rev. Chem. Biomol. Eng. **2**, 147 (2011).
[3] L. R. Pratt, Annu. Rev. Phys. Chem. **53**, 409 (2002).
[4] D. Chandler, Nature (London) **437**, 640 (2005).
[5] M. B. Hillyer and B. C. Gibb, Annu. Rev. Phys. Chem. **67**, 307 (2016).
[6] D. Ben-Amotz, Annu. Rev. Phys. Chem. **67**, 617 (2016).
[7] S. X. Cui, Acta Polym. Sin. 1160 (2016).
[8] E. Brini, C. J. Fennell, M. Fernandez-Serra, B. Hribar-Lee, M. Luksic, and K. A. Dill, Chem. Rev. **117**, 12385 (2017).
[9] F. H. Stillinger, J. Solution Chem. **2**, 141 (1973).
[10] K. Lum, D. Chandler, and J. D. Weeks, J. Phys. Chem. B **103**, 4570 (1999).
[11] D. M. Huang, P. L. Geissler, and D. Chandler, J. Phys. Chem. B **105**, 6704 (2001).
[12] D. M. Huang and D. Chandler, J. Phys. Chem. B **106**, 2047 (2002).
[13] M. V. Athawale, S. N. Jamadagni, and S. Garde, J. Chem. Phys. **131**, 115102 (2009).
[14] R. G. Weiß, M. Heyden, and J. Dzubiella, Phys. Rev. Lett. **114**, 187802 (2015).
[15] P. R. ten Wolde and D. Chandler, Proc. Natl. Acad. Sci. U.S.A. **99**, 6539 (2002).
[16] D. M. Huang and D. Chandler, Proc. Natl. Acad. Sci. U.S.A. **97**, 8324 (2000).
[17] S. Rajamani, T. M. Truskett, and S. Garde, Proc. Natl. Acad. Sci. U.S.A. **102**, 9475 (2005).
[18] R. L. Baldwin, FEBS Lett. **587**, 1062 (2013).
[19] Y. Nozaki and C. Tanford, J. Biol. Chem. **246**, 2211 (1971).
[20] R. L. Baldwin, Proc. Natl. Acad. Sci. U.S.A. **110**, 1670 (2013).
[21] R. L. Baldwin and G. D. Rose, Proc. Natl. Acad. Sci. U.S.A. **113**, 12462 (2016).
[22] J. G. Davis, K. P. Gierszal, P. Wang, and D. Ben-Amotz, Nature (London) **491**, 582 (2012).
[23] I. T. S. Li and G. C. Walker, J. Am. Chem. Soc. **132**, 6530 (2010).
[24] I. T. S. Li and G. C. Walker, Proc. Natl. Acad. Sci. U.S.A. **108**, 16527 (2011).
[25] I. T. S. Li and G. C. Walker, Acc. Chem. Res. **45**, 2011 (2012).
[26] J. Mondal, D. Halverson, I. T. S. Li, G. Stirnemann, G. C. Walker, and B. J. Berne, Proc. Natl. Acad. Sci. U.S.A. **112**, 9270 (2015).
[27] V. R. Agashe, M. C. R. Shastry, and J. B. Udgaonkar, Nature (London) **377**, 754 (1995).
[28] R. H. Zhou, X. H. Huang, C. J. Margulis, and B. J. Berne, Science **305**, 1605 (2004).
[29] See Supplemental Material at [http://link.aps.org/supplemental/10.1103/PhysRevLett.122.047801 to be inserted by publisher] for further details on experiments and methods, which includes Refs. [30–41].
[30] K. J. Zhou, J. F. Li, Y. J. Lu, G. Z. Zhang, Z. W. Xie, and C. Wu, Macromolecules **42**, 7146 (2009).
[31] Q. Sun and R. Faller, Macromolecules **39**, 812 (2006).

[32] M. Pütz, K. Kremer, and G. S. Grest, Europhys. Lett. **49**, 735 (2000).
[33] R. S. Hoy, K. Foteinopoulou, and M. Kröger, Phys. Rev. E **80**, 031803 (2009).
[34] R. Everaers, S. K. Sukumaran, G. S. Grest, C. Svaneborg, A. Sivasubramanian, and K. Kremer, Science **303**, 823 (2004).
[35] A. Nikoubashman, V. E. Lee, C. Sosa, R. K. Prud'homme, R. D. Priestley, and A. Z. Panagiotopoulos, ACS Nano **10**, 1425 (2016).
[36] T. I. Morozova and A. Nikoubashman, J. Phys. Chem. B **122**, 2130 (2018).
[37] S. A. Chizhik, Z. Huang, V. V. Gorbunov, N. K. Myshkin, and V. V. Tsukruk, Langmuir **14**, 2606 (1998).
[38] B. J. Briscoe, L. Fiori, and E. Pelillo, J. Phys. D **31**, 2395 (1998).
[39] H.-Y. Nie, M. Motomatsu, W. Mizutani, and H. Tokumoto, J. Vac. Sci. Technol. B **13**, 1163 (1995).
[40] S. Tan, R. L. Sherman, and W. T. Ford, Langmuir **20**, 7015 (2004).
[41] D. Guo, J. N. Li, G. X. Xie, Y. Y. Wang, and J. B. Luo, Langmuir **30**, 7206 (2014).
[42] J. F. Marko and E. D. Siggia, Macromolecules **28**, 8759 (1995).
[43] A. Nikoubashman, V. E. Lee, C. Sosa, R. K. Prud'homme, R. D. Priestley, and A. Z. Panagiotopoulos, ACS Nano **10**, 1425 (2016).
[44] T. I. Morozova and A. Nikoubashman, J. Phys. Chem. B **122**, 2130 (2018).
[45] F. P. Buff, R. A. Lovett, and F. H. Stillinger, Phys. Rev. Lett. **15**, 621 (1965).
[46] J. Mittal and G. Hummer, Proc. Natl. Acad. Sci. U.S.A. **105**, 20130 (2008).